A Distributed Circuit Model for Side-Coupled Nanoplasmonic Structures With Metal–Insulator–Metal Arrangement

Mohsen Rezaei, Sadegh Jalaly, Mehdi Miri, Amin Khavasi, Ali P. Fard, Khashayar Mehrany, and Bizhan Rashidian

***Abstract*—A transmission line model is developed for coupled plasmonic metal–insulator–metal (MIM) waveguides. In the proposed model coupling between electric fields of two plasmonic waveguides is modeled by distributed mutual capacitor while distributed mutual inductor accounts for magnetic field coupling. These mutual elements are determined using propagation constants of supermodes of coupled waveguides. The model is applied to analyze coupled line directional coupler and side-coupled rectangular resonators. The effectiveness of the model is assessed using fully numerical finite-difference time-domain (FDTD) technique. The results have excellent agreement with the numerical methods.**

***Index Terms*—Directional couplers, equivalent circuits, optical waveguides, plasmons, parallel plate waveguides.**

I. Introduction

PLASMONICS is receiving a considerable and growing attention as a promising technology to overcome the diffraction limit for miniaturization of photonic circuits down to nanometric dimensions [1], [2]. Miscellaneous topologies and arrangements have hitherto been proposed to realize plasmonic oscillations in metallic structures, viz., V-grooves in metal substrate [3], metallic nanowires [4], metallic nanoparticle arrays [5], and planar metal–insulator–metal (MIM) structures [6]. Thanks to the beneficent electromagnetic properties of the latter arrangement, e.g., very strong field localization, and almost-zero bending loss, MIM structures are among the most favorable. It is, therefore, no surprise that different types of nanoscale photonic devices, filters [7], [8], switches [9], [10], couplers [10]–[12], and demultiplexers [12], [13]—just to name a few, are based on the MIM arrangement. These structures are usually fabricated by deposition of noble metals on fused dielectric substrates [14], [15].

Given that all these devices have subwavelength features, numerical methods for rigorous electromagnetic analysis are burdensome to be applied. Therefore, the availability of accurate enough approximate methods in electromagnetic analysis of such devices is indeed welcome. Transmission line models, in particular, have enjoyed recent popularity in fast yet accurate enough modeling of a variety of plasmonic devices [16]–[22]. They bring the concepts and standard design methodologies of microwave engineering to plasmonics and thereby improve our design ability.

It is fortunate that the transmission line model conforms straightforwardly to the MIM arrangement, which—as it was already mentioned, happens to be quite popular. MIM waveguide with stubs [17], [18], power dividers [19], subwavelength frequency splitter [13], waveguide discontinuities [20], filters [21], absorption switches [11], and resonators [22] are all already modeled by transmission lines. No attempt is, however, made to apply the transmission line model for analysis of side-coupled plasmonic devices like MIM directional couplers [10]–[12], and side-coupled resonators [7], etc. This is due to the fact that the transmission line in all of the already reported models is always a single conductor line, which cannot take the effects of coupling into account.

Here, for the first time to the best of our knowledge, a multiconductor transmission line is introduced to account for the coupling effects in MIM structures, and thus, a distributed circuit model is proposed for analysis of side-coupled plasmonic structures. The electrical characteristics of the multiconductor transmission line in the proposed model are given by closed-form expressions in terms of easily extractable parameters; namely, the propagation constants of appropriate MIM waveguides whose geometries depend on the structure under study.

This paper is organized as follows: first, the multiconductor transmission line model is introduced and its parameters are extracted in Section II. The proposed distributed circuit model is then applied for analysis of two typical side-coupled MIM devices, viz., directional couplers and side-coupled resonators. The proposed model is then justified by the well-known finite-difference time-domain (FDTD) method in Section III. Finally, the conclusions are made in Section IV.

II. Multiconductor Transmission Line Model for Coupling in MIMs

The coupling mechanism in side-coupled plasmonic devices with MIM arrangement can be studied by a distributed circuit if a multiconductor transmission line model is developed to account for the electromagnetic wave coupling between adjacent MIM waveguides, which exist in the device. This is performed here by considering a simple structure made of two parallel MIM waveguides. This structure is schematically shown in Fig. 1(a) and can be modeled by a two-conductor transmission line shown in Fig. 1(b). Once the electromagnetic coupling

Manuscript received December 27, 2011; revised March 3, 2012; accepted March 4, 2012.

The authors are with the Electrical Engineering Department, Sharif University of Technology, Tehran 1155-4363, Iran (e-mail: mrezaei86@ee.sharif.edu; sadeghjalaly@gmail.com; m101miri@gmail.com; amin_xavasi@yahoo.com; apyfrd@gmail.com; mehrany@sharif.edu; rashidia@sharif.edu).

Color versions of one or more of the figures in this paper are available online at http://ieeexplore.ieee.org.

Digital Object Identifier 10.1109/JSTQE.2012.2190267

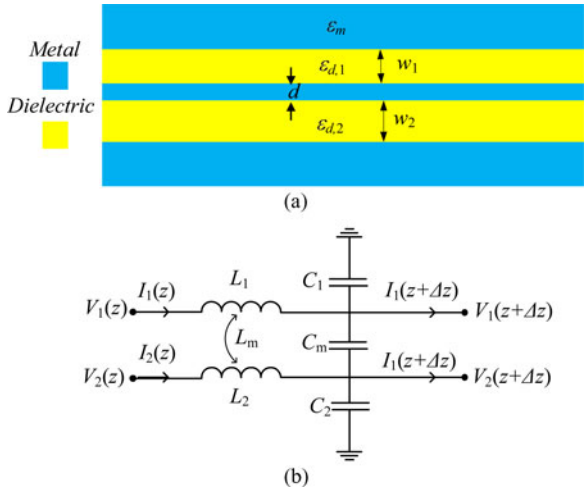

Fig. 1. (a) Schematic diagram of coupled MIM plasmonic waveguides. (b) Corresponding coupled transmission line model.

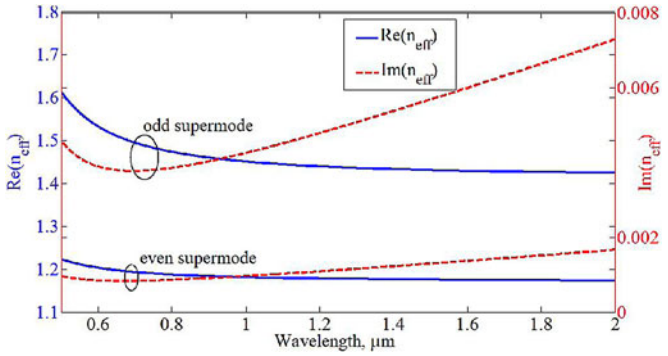

Fig. 2. Effective refractive indices of even and odd supermodes versus the wavelength of light at free space. The geometrical parameters are in accordance with Fig. 1: $w_1 = 60\,\text{nm}$, $w_2 = 10\,\text{nm}$, and $d = 20\,\text{nm}$.

in this structure is successfully taken into account, different types of side-coupled plasmonic devices, e.g., directional coupler and side-coupled waveguide-resonator, can be straightforwardly modeled by using an appropriately loaded two-conductor transmission line shown in Fig. 1(b). This is demonstrated in the next section, where distributed circuits based on two-conductor transmission lines are given for modeling directional couplers and side-coupled waveguide-resonators.

In the sought-after two-conductor transmission line model—which is schematically shown in Fig. 1(b), L_1,C_1 and L_2,C_2 denote the self-inductance and self-capacitance of the upper and lower MIM waveguides, respectively. The upper waveguide has a dielectric layer of width w_1 and permittivity $\varepsilon_{d,1}$ which is carved in a metallic region of permittivity ε_m. The width of the lower waveguide is w_2 and its dielectric permittivity is $\varepsilon_{d,2}$. The electromagnetic coupling between these two waveguides is in this model represented by a mutual capacitance C_m and a mutual inductance L_m. The proposed two-conductor transmission line model is, therefore, determined when all of the abovementioned parameters, viz., L_1, C_1, L_2, C_2, L_m, C_m, are found.

Finding all of the abovementioned parameters from scratch is a burdensome task; therefore, the physical meaning of each of the parameters can be evoked to have them obtained more straightforwardly. The mutual inductance; L_m and the mutual capacitance; C_m are expected to account for the coupling effects; therefore, the remaining parameters L_1, C_1, L_2, and C_2 can be obtained by studying wave propagation in the standard single conductor transmission lines representing the upper and lower waveguides separately. This proves to be a good approximation because the effects of self-inductance and self-capacitance are minimal on the coupling. Fortunately, extraction of the self-inductance and the self-capacitance of a standard single conductor transmission line modeling a typical MIM waveguide is an undemanding task. The details are given in the Appendix I, where L_1, C_1, L_2, and C_2 are shown to be

$$L_1 = \frac{\beta_{w1}^2}{\omega^2 \varepsilon_0 \varepsilon_{d,1}} \tag{1a}$$

$$C_1 = \varepsilon_0 \varepsilon_{d,1} \tag{1b}$$

$$L_2 = \frac{\beta_{w2}^2}{\omega^2 \varepsilon_0 \varepsilon_{d,2} d} \tag{1c}$$

$$C_2 = \varepsilon_0 \varepsilon_{d,2} d. \tag{1d}$$

In these expressions, β_{w1} and β_{w2} stand for the propagation constants of the upper and lower waveguides, respectively. Given that β_{w1} and β_{w2} are complex numbers for lossy structures, the self-inductance of the line is usually complex and has a series resistance. The self-capacitance, on the other hand, is complex and has a shunt conductance only if the dielectric permittivity is complex, which is not the case when the dielectric is air.

To obtain the remaining parameters, L_m and C_m, the propagation constants of the supermodes of the coupled MIM waveguides (upper and lower waveguides together) are employed. These supermode propagation constants are hereafter denoted by β_e, and β_o for the even and odd mode profiles, respectively. They can be easily extracted by using any of the standard mode extraction methods already reported for multilayer waveguides [23]. As an example, it is assumed that the parameters of the typical structure shown in Fig. 1(a) is $w_1 = 60\,\text{nm}$, $w_2 = 100\,\text{nm}$, and $d = 20\,\text{nm}$, when the metallic and dielectric regions are silver and air, respectively. The effective refractive indices of the even and odd propagation constants of this typical structure are plotted versus the free space wavelength; λ_0 in Fig. 2 (the effective refractive index is $n_{\text{eff}} = \beta\lambda_0/2\pi$ if β is the propagation constant).

To demonstrate that the yet unknown L_m and C_m can be related to the even and odd propagation constants of the structure, the telegrapher's equations for the two-conductor transmission line shown in Fig. 1(b) is needed

$$\frac{\partial}{\partial z}\begin{bmatrix} V_1 \\ V_2 \end{bmatrix} = -j\omega \mathbf{L} \begin{bmatrix} I_1 \\ I_2 \end{bmatrix} \tag{2a}$$

$$\frac{\partial}{\partial z}\begin{bmatrix} I_1 \\ I_2 \end{bmatrix} = -j\omega \mathbf{C} \begin{bmatrix} V_1 \\ V_2 \end{bmatrix}. \tag{2b}$$

Here, V_1, I_1 and V_2, I_2 represent the voltage and current of lines 1 and 2, respectively, and we have

$$\mathbf{L} = \begin{bmatrix} L_1 & L_m \\ L_m & L_2 \end{bmatrix} \tag{3a}$$

$$\mathbf{C} = \begin{bmatrix} C_1 + C_m & -C_m \\ -C_m & C_2 + C_m \end{bmatrix}. \tag{3b}$$

It is straightforward to show that

$$\frac{\partial^2}{\partial z^2} \begin{bmatrix} V_1 \\ V_2 \end{bmatrix} = -\omega^2 \boldsymbol{\chi}_V \begin{bmatrix} V_1 \\ V_2 \end{bmatrix} \tag{4a}$$

$$\frac{\partial^2}{\partial z^2} \begin{bmatrix} I_1 \\ I_2 \end{bmatrix} = -\omega^2 \boldsymbol{\chi}_I \begin{bmatrix} I_1 \\ I_2 \end{bmatrix} \tag{4b}$$

where $\chi_V = \mathbf{LC}$ and $\chi_I = \mathbf{CL}$.

Since the diagonalization of the $\boldsymbol{\chi}_V$ and $\boldsymbol{\chi}_I$ matrices uncouples the voltage–current distribution of line 1 from that of the line 2, the governing equations of the voltages and currents of the even and odd supermodes—whose propagation constants are assumed to be known, can be written as

$$\frac{\partial^2}{\partial z^2} \begin{bmatrix} V_e \\ V_o \end{bmatrix} = -\omega^2 \mathbf{D} \begin{bmatrix} V_e \\ V_o \end{bmatrix} \tag{5a}$$

$$\frac{\partial^2}{\partial z^2} \begin{bmatrix} I_e \\ I_o \end{bmatrix} = -\omega^2 \mathbf{D} \begin{bmatrix} I_e \\ I_o \end{bmatrix} \tag{5b}$$

where

$$\begin{bmatrix} V_e \\ V_o \end{bmatrix} = \mathbf{Q}_V^{-1} \begin{bmatrix} V_1 \\ V_2 \end{bmatrix} \tag{6a}$$

$$\begin{bmatrix} I_e \\ I_o \end{bmatrix} = \mathbf{Q}_I^{-1} \begin{bmatrix} I_1 \\ I_2 \end{bmatrix}. \tag{6b}$$

$\boldsymbol{\chi}_V$ and $\boldsymbol{\chi}_I$ in these expressions are written as

$$\boldsymbol{\chi}_V = \mathbf{Q}_V \mathbf{D} \mathbf{Q}_V^{-1} \tag{7a}$$

and

$$\boldsymbol{\chi}_I = \mathbf{Q}_I \mathbf{D} \mathbf{Q}_I^{-1} \tag{7b}$$

where $\mathbf{D}$, $\mathbf{Q}_V$, and $\mathbf{Q}_I$ are the eigenvalue and eigenvectors matrices of $\boldsymbol{\chi}_V$, and $\boldsymbol{\chi}_I$, matrices, respectively,

$$\mathbf{D} = \begin{bmatrix} \zeta_e & 0 \\ 0 & \zeta_o \end{bmatrix} \tag{8a}$$

$$\mathbf{Q}_V = \begin{bmatrix} \mathbf{Q}_{Ve} & \mathbf{Q}_{Vo} \end{bmatrix} \tag{8b}$$

$$\mathbf{Q}_I = \begin{bmatrix} \mathbf{Q}_{Ie} & \mathbf{Q}_{Io} \end{bmatrix}. \tag{8c}$$

In view of the fact that V_e, I_e and V_o, I_o are now uncoupled, the corresponding eigenvalues of the even and odd eigenvectors, i.e., ζ_e and ζ_o, are related to the propagation constants of the even and odd supermodes, i.e., β_e, and β_o, respectively,

$$\zeta_e = \left(\frac{\beta_e}{\omega}\right)^2 \tag{9a}$$

$$\zeta_o = \left(\frac{\beta_o}{\omega}\right)^2. \tag{9b}$$

Now, since the eigenvalues of the $\boldsymbol{\chi}_V$ and $\boldsymbol{\chi}_I$ matrices are known in terms of the model parameters—which include the yet unknown L_m and C_m, we can use (9a) and (9b) to obtain L_m and C_m by using the already determined $L_1, C_1, L_2, C_2, \beta_e, \beta_o$, and ω. It is straightforward to show that L_m is as follows:

$$L_m = g_0 - \sqrt{g_0^2 + g_1} \tag{10a}$$

where

$$g_0 = \frac{1}{4C_1C_2}\left(\frac{(C_1 + C_2)(\beta_e^2 + \beta_o^2)}{\omega^2} - L_1C_1^2 - L_2C_2^2\right) - \left(\frac{L_1 + L_2}{4}\right) \tag{10b}$$

$$g_1 = L_1L_2 - \frac{(\beta_e\beta_o)^2}{C_1C_2\omega^4} + \frac{L_1L_2(C_1 + C_2)}{C_1C_2(L_1 + L_2)} \times \left(\frac{\beta_e^2 + \beta_o^2}{\omega^2} - L_1C_1 - L_2C_2\right). \tag{10c}$$

The mutual capacitance between the two conductors of the line is then

$$C_m = \frac{1}{L_1 + L_2 - 2L_m}\left(\frac{\beta_e^2 + \beta_o^2}{\omega^2} - L_1C_1 - L_2C_2\right). \tag{11}$$

Substitution of the abovementioned L_m and C_m in the $\boldsymbol{\chi}_V$ or $\boldsymbol{\chi}_I$ matrices gives the appropriate set of eigenvalues ζ_e and ζ_o. As expected, the eigenvectors associated with the, thus, obtained set of eigenvalues are lying in the correct quadrants (The first/third and the second/forth quadrants for the even and odd eigenvectors, $\mathbf{Q}_e$ and $\mathbf{Q}_o$, respectively).

Now that all the per-unit-length circuit elements are determined in terms of easy-to-obtain parameters—i.e., MIM waveguide propagation constants: β_1, β_2, β_e, and β_o, the even and odd characteristic impedances of the proposed two-conductor transmission line can be easily extracted by substituting (6) in (2) and then by carrying out simple algebraic manipulations to show that

$$\frac{\partial}{\partial z} \begin{bmatrix} V_e \\ V_o \end{bmatrix} = -j\omega \mathbf{P} \begin{bmatrix} I_e \\ I_o \end{bmatrix} \tag{12a}$$

$$\frac{\partial}{\partial z} \begin{bmatrix} I_e \\ I_o \end{bmatrix} = -j\omega \mathbf{R} \begin{bmatrix} V_e \\ V_o \end{bmatrix} \tag{12b}$$

where

$$\mathbf{P} = [p_{ij}]_{2\times 2} = \mathbf{Q}_V^{-1}\mathbf{L}\mathbf{Q}_I \tag{13a}$$

$$\mathbf{R} = [r_{ij}]_{2\times 2} = \mathbf{Q}_I^{-1}\mathbf{C}\mathbf{Q}_V. \tag{13b}$$

The uncoupled nature of even and odd voltage and current distributions implies the diagonality of the $\mathbf{P}$ and $\mathbf{R}$ matrices in (12). It should be, however, noted that the off-diagonal elements of these matrices are in fact nonzero, when the obtained per-unit-length circuit elements are substituted in $\boldsymbol{\chi}_V$ and $\boldsymbol{\chi}_I$. This is due to the fact that the self-inductance and self-capacitance of the line was calculated without taking the effects of coupling between

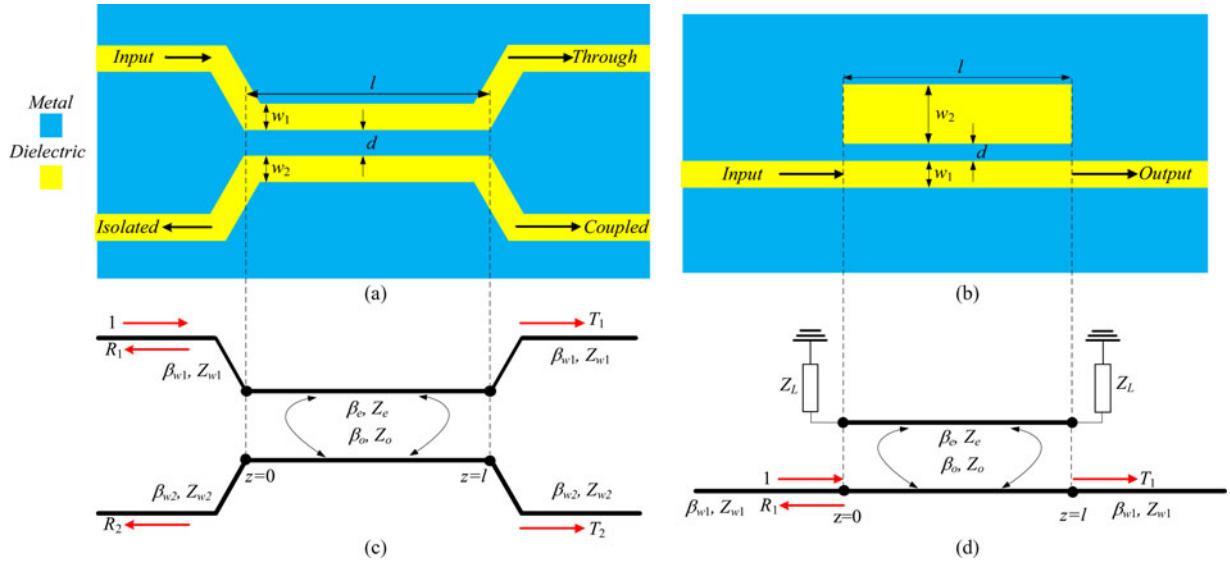

Fig. 3. Schematic view of: (a) MIM coupled line directional coupler. (b) Side-coupled waveguide-resonator. (c) Proposed transmission line model employed for analysis of the MIM coupled line directional coupler. (d) Side-coupled waveguide-resonator.

the lines into account, i.e., they are based on β_1, and β_2 rather than supermode propagation constants β_e and β_o. It is fortunate that this approximation is insignificant since the off-diagonal elements of the **P** and **R** matrices are negligible in comparison with the diagonal elements. It can be easily shown that

$$Z_e = \sqrt{\frac{p_{11}}{r_{11}}} \tag{14}$$

and

$$Z_o = \sqrt{\frac{p_{22}}{r_{22}}} \tag{15}$$

are the even and odd characteristic impedances, respectively.

III. Applications in Analysis of Side-Coupled MIM Structures

In this section, the proposed two-conductor transmission line model is applied to analyze side-coupled plasmons in two typical plasmonic structures. One is a standard coupled line directional coupler [10] shown in Fig. 3(a). The other is the well-known side-coupled waveguide-resonator structure [7] shown in Fig. 3(b). Both are made by carving empty regions within silver. While it is clear that the permittivity of the dielectric region is $\varepsilon_d = 1$ for the empty regions, the complex permittivity of the metallic region is estimated by using the well-known Drude model [22]

$$\varepsilon_m(\omega) = \varepsilon_\infty - \frac{\omega_p^2}{\omega(\omega - j\gamma)} \tag{16}$$

where the bulk plasma frequency, the collision rate, and the permittivity at infinite frequency are set to $\omega_p = 1.38 \times 10^{16}$ Hz, $\gamma = 2.73 \times 10^{13}$ Hz, and $\varepsilon_\infty = 3.7$, respectively.

The proposed transmission line models for these two typical devices are schematically shown in Fig. 3(c) and (d). For simplicity's sake, the ground conductor is not shown in the sketch. The obtained results are then validated by using the standard FDTD method.

A. Coupled Line Directional Coupler

Plasmonic coupled line directional coupler is the most straightforward device to be analyzed by employing the proposed model. This is demonstrated in this section, where the proposed model is employed to calculate how much of the input power is fed to the coupled, through and isolated ports. The upper waveguide is modeled by a single conductor transmission line whose propagation constant and characteristics impedance are β_{w1} and Z_{w1}, respectively. In accordance with the Appendix I, the latter can be written in terms of the former

$$Z_{w1} = \frac{\beta_{w1}}{\omega\varepsilon_0\varepsilon_d}. \tag{17}$$

In a similar fashion, the lower waveguide is modeled by a single conductor transmission line whose propagation constant and characteristics impedance are β_{w2} and Z_{w2}. In a similar fashion, we have

$$Z_{w2} = \frac{\beta_{w2}}{\omega\varepsilon_0\varepsilon_d}. \tag{18}$$

Neglecting the bending effects, the cross-talk between the upper and lower waveguides can now be easily modeled by following the proposed strategy to calculate the mutual inductance; L_m and capacitance; C_m [see Fig. 3(c)]. Once the per-unit-length circuit parameters are extracted, the transmission and reflection spectrum of the structure can be analytically obtained in accordance with the Appendix II.

Two different cases are considered. First, it is assumed that the thickness of both waveguides are $w_1 = w_2 = 60$ nm, the geometrical length of the coupler is $l = 1.2$ μm, and the distance between the upper and lower waveguides are $d = 20$ nm. The power spectrum at the coupled and through ports is then calculated by using the proposed model, and the FDTD method with

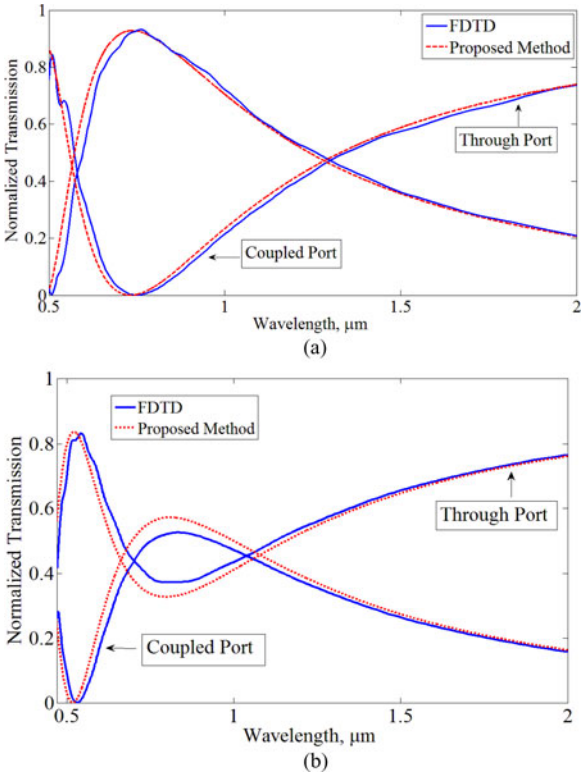

Fig. 4. (a) Power spectrum at the coupled and through ports of a typical symmetric directional coupler with $w_1 = 60\,\text{nm}$, $w_2 = 60\,\text{nm}$, $d = 20\,\text{nm}$, and $l = 1.2\ \mu\text{m}$: the FDTD method (solid line), and the proposed circuit model (dashed line). (b) Power spectrum at the coupled and through ports of a typical asymmetric directional coupler with: $w_1 = 60\,\text{nm}$, $w_2 = 100\,\text{nm}$, $d = 28\,\text{nm}$, and $l = 2\ \mu\text{m}$: the FDTD method (solid line), and the proposed circuit model (dashed line).

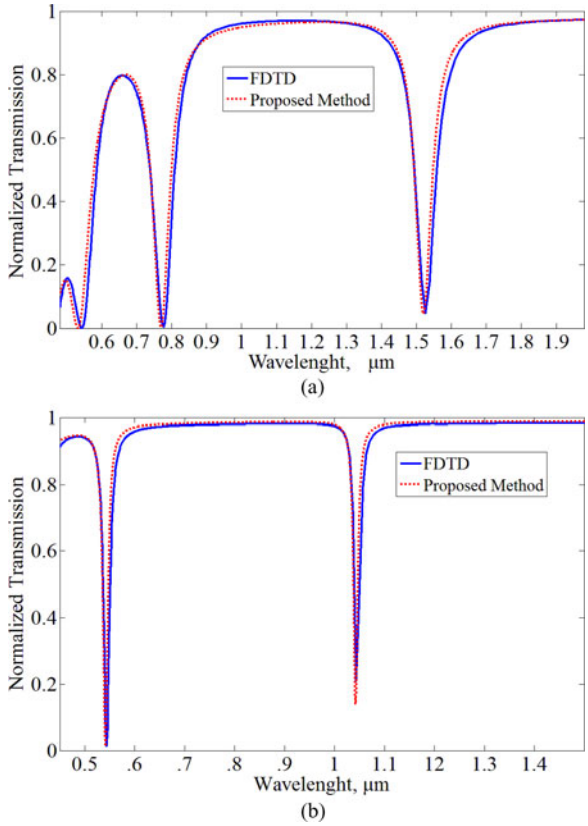

Fig. 5. (a) Transmission spectrum of a side-coupled resonator with $w_1 = 50\,\text{nm}$, $w_2 = 50\,\text{nm}$, $h = 20\,\text{nm}$, and $d = 500\,\text{nm}$ [7]: the FDTD results (solid line), and the proposed circuit model (dashed line). (b) Transmission spectrum of a side-coupled resonator with $w_1 = 60\,\text{nm}$, $w_2 = 120\,\text{nm}$, $h = 32\,\text{nm}$, and $l = 400\,\text{nm}$: the FDTD results and (solid line), the proposed method (dashed line).

the grid size of 4 nm × 4 nm. The results are plotted in Fig. 4(a). A very good agreement is observed between the results obtained by the proposed simple model and the rigorous FDTD method. Second, it is assumed that $w_1 = 60\,\text{nm}$ and $w_2 = 100\,\text{nm}$, i.e., the structure is asymmetric. The power spectrum at the coupled and through ports is once again calculated when $d = 28\,\text{nm}$ and $l = 2\ \mu\text{m}$. The results are plotted in Fig. 4(b), where the proposed transmission line model is justified by the FDTD method.

B. Side-Coupled Waveguide-Resonator

Although not as straightforward as in the previous case of directional couplers, the proposed transmission line model can still be employed to analyze side-coupled waveguide-resonator structures. Dielectric rectangular cavities carved in metals are already modeled by using a single conductor standard transmission line [22]. Given that MIM waveguides are also modeled by the single conductor standard transmission line, the effects of side-coupling between MIM waveguides and rectangular cavities can be taken into account. This is shown schematically in Fig. 3(d), where the side coupling is modeled by the crosstalk between the terminated transmission line representing the rectangular cavity and the transmission line representing the MIM waveguide.

The scalar impedance terminating the transmission line in modeling of the rectangular cavity is already obtained [17]

$$Z_L = \sqrt{\frac{\varepsilon_d}{\varepsilon_m}} Z_{w2} \tag{19}$$

where Z_{w2} is introduced in (21). The mutual capacitance and inductance between the two transmission lines representing the cavity and the waveguide are then extracted by using the proposed strategy. The details are presented in Appendix III.

As the first numerical example, and in accordance with Fig. 3(b), we have $w_1 = w_2 = 50\,\text{nm}$, $h = 20\,\text{nm}$, and $d = 500\,\text{nm}$. The transmission spectrum of the structure is then shown in Fig. 5(a), where the proposed transmission line model is justified by the FDTD method. The grid size of the FDTD scheme is 2 nm × 2 nm.

As the final example, we set $w_1 = 60\,\text{nm}$, $w_2 = 120\,\text{nm}$, $l = 400\,\text{nm}$, and $d = 32\,\text{nm}$. This time the two-conductor transmission line is asymmetric. Yet, the side-coupling mechanism is successfully considered and transmission spectrum of the structure is plotted in Fig. 5(b). Once again, the proposed model has a good agreement with the FDTD method.

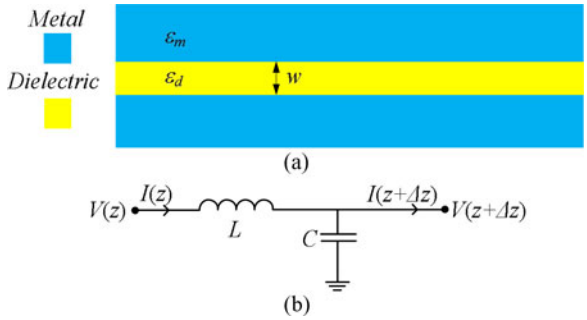

Fig. 6. (a) Typical MIM waveguide. (b) Its distributed circuit model.

IV. Conclusion

In conclusion, a transmission line model is developed to model side coupling in plasmonic devices with MIM arrangement. The proposed model is based on two-conductor transmission line and requires nothing, but the easy to extract propagation constants of the coupled and uncoupled MIM waveguides in the structure. The proposed model can be used in design of different types of plasmonic devices, whenever there is a side coupling between plasmons in the MIM arrangement.

The model works properly in so far as the higher order modes of the waveguides remain evanescent.

Appendix I

Consider a typical metal–insulator–metal waveguide shown in Fig. 6(a). A simple distributed lumped circuit model for this waveguide is a single conductor standard transmission line shown in Fig. 6(b).

On one hand, the ratio of the transverse electric field to the transverse magnetic field in this waveguide can be approximated by using the impedance of the parallel plate waveguide

$$Z_w = \frac{\beta_w}{\omega \varepsilon_0 \varepsilon_d} \tag{A1}$$

where ε_d and β_w are the permittivity of the dielectric region, and the propagation constant of the MIM waveguide, respectively.

On the other hand, the standard transmission line theory relates the propagation constant and the characteristic impedance of the line to its self-inductance and capacitance

$$\beta = \omega\sqrt{LC} \tag{A2}$$

$$Z_0 = \sqrt{\frac{L}{C}}. \tag{A3}$$

The per-unit-length self-inductance and capacitance of the line can then be easily obtained by combining (A1), (A2), and (A3)

$$C = \varepsilon_0 \varepsilon_d \tag{A4}$$

$$L = \frac{\beta^2}{\omega^2 \varepsilon_0 \varepsilon_d}. \tag{A5}$$

It is worth noting that while the self-inductance L is always complex because the propagation constant of the line is determined in terms of the complex metallic permittivity, the self-capacitance is real for real ε_d, i.e., when the dielectric region is lossless.

Appendix II

In accordance with Fig. 3(c), the voltage and current distributions of the upper and lower transmission lines read as

$$\begin{pmatrix} \mathbf{V} \\ \mathbf{I} \end{pmatrix} = \begin{pmatrix} V_1 \\ V_2 \\ I_1 \\ I_2 \end{pmatrix} = \begin{pmatrix} e^{-j\beta_{w1}z} + R_1 e^{j\beta_{w1}z} \\ R_2 e^{j\beta_{w2}z} \\ \left(e^{-j\beta_{w1}z} - R_2 e^{j\beta_{w1}z}\right)/Z_{w1} \\ \left(-R_2 e^{j\beta_{w2}z}\right)/Z_{w2} \end{pmatrix} \tag{A6}$$

for $z < 0$, and

$$\begin{pmatrix} \mathbf{V} \\ \mathbf{I} \end{pmatrix} = \begin{pmatrix} T_1 e^{-j\beta_{w1}(z-l)} \\ T_2 e^{-j\beta_{w2}(z-l)} \\ T_1 e^{-j\beta_{w1}(z-l)}/Z_{w1} \\ T_2 e^{-j\beta_{w2}(z-l)}/Z_{w2} \end{pmatrix} \tag{A7}$$

for z $> l$.

The transmission and reflection spectra of the upper and lower transmission lines; R_1, R_2, T_1, and T_2, can now be straightforwardly extracted once the following set of equations obtained by combining (2a) and (2b) is solved

$$\frac{\partial}{\partial z}\begin{bmatrix} \mathbf{V} \\ \mathbf{I} \end{bmatrix} = \mathbf{G}\begin{bmatrix} \mathbf{V} \\ \mathbf{I} \end{bmatrix} \tag{A8}$$

$$\mathbf{G} = \begin{pmatrix} \mathbf{0} & -j\omega\mathbf{L} \\ -j\omega\mathbf{C} & \mathbf{0} \end{pmatrix}. \tag{A9}$$

Since the kernel matrix of the preceding set of equations; $\mathbf{G}$ is not a function of z, we have

$$\begin{pmatrix} \mathbf{V}(l) \\ \mathbf{I}(l) \end{pmatrix} = \exp(\mathbf{G}l)\begin{pmatrix} \mathbf{V}(0) \\ \mathbf{I}(0) \end{pmatrix}. \tag{A10}$$

The transfer matrix exp($\mathbf{G}l$) can now be partitioned as follows:

$$\exp(\mathbf{G}l) = \begin{pmatrix} \mathbf{W}_{11} & \mathbf{W}_{12} \\ \mathbf{W}_{21} & \mathbf{W}_{22} \end{pmatrix} \tag{A11}$$

and the unknown transmission and reflection spectra are easily found

$$\begin{pmatrix} \mathbf{T} \\ \mathbf{R} \end{pmatrix} = \begin{pmatrix} \mathbf{1} & -\mathbf{W}_{11} + \mathbf{W}_{12}\mathbf{Y}_1 \\ \mathbf{Y}_1 & -\mathbf{W}_{21} + \mathbf{W}_{22}\mathbf{Y}_1 \end{pmatrix}^{-1} \exp(\mathbf{G}l)\mathbf{D} \tag{A12}$$

where

$$\mathbf{T} = \begin{bmatrix} T_1 \\ T_2 \end{bmatrix} \tag{A13}$$

$$\mathbf{R} = \begin{bmatrix} R_1 \\ R_2 \end{bmatrix} \tag{A14}$$

$$\mathbf{Y}_1 = \begin{bmatrix} 1/Z_{w1} & 0 \\ 0 & 1/Z_{w2} \end{bmatrix} \tag{A15}$$

$$\mathbf{D} = \begin{bmatrix} 1 \\ 0 \\ 1/Z_{w1} \\ 0 \end{bmatrix}. \tag{A16}$$

APPENDIX III

In accordance with Fig. 3(d), the voltage and current distributions of the upper and lower transmission lines read as

$$\begin{pmatrix} \mathbf{V} \\ \mathbf{I} \end{pmatrix} == \begin{pmatrix} 1+\mathrm{R} \\ V_2(0) \\ (1-\mathrm{R})/Z_{w1} \\ -V_2(0)/Z_L \end{pmatrix} \tag{A17}$$

at $z = 0$, and

$$\begin{pmatrix} \mathbf{V} \\ \mathbf{I} \end{pmatrix} == \begin{pmatrix} T \\ V_2(l) \\ T/Z_{w1} \\ V_2(l)/Z_L \end{pmatrix} \tag{A18}$$

at $z = l$.

Along the same line, the unknown transmission and reflection spectra can be easily written as

$$\begin{pmatrix} R \\ V_2(0) \\ T \\ V_2(l) \end{pmatrix} = \begin{pmatrix} \mathbf{1} & -\mathbf{W}_{11} + \mathbf{W}_{12}\mathbf{Y}_2 \\ \mathbf{Y}_2 & -\mathbf{W}_{21} + \mathbf{W}_{22}\mathbf{Y}_2 \end{pmatrix}^{-1} \exp(\mathbf{G}l)\mathbf{D} \tag{A19}$$

where

$$\mathbf{Y}_2 = \begin{bmatrix} 1/Z_{w1} & 0 \\ 0 & 1/Z_L \end{bmatrix}. \tag{A20}$$

REFERENCES

[1] E. Ozbay, "Plasmonics: Merging photonics and electronics at nanoscale dimensions," *Science*, vol. 311, pp. 570–578, Jan. 2006.

[2] D. K. Gramotnev and S. I. Bozhevolnyi, "Plasmonics beyond the diffraction limit," *Nature Photon.*, vol. 4, pp. 83–91, Feb. 2010.

[3] S. I. Bozhevolnyi, V. S. Volkov, E. Devaux, and T. W. Ebbesen, "Channel Plasmon-polariton guiding by subwavelength metal grooves," *Phys. Rev. Lett.*, vol. 95, pp. 046802-1–046802-3, Jul. 2005.

[4] V. A. Podolskiy, A. K. Sarychev, and V. M. Shalaev, "Plasmon modes and negative refraction in metal nanowire composites," *Optics Express*, vol. 11, pp. 735–745, Mar. 2003.

[5] S. A. Maier, P. G. Kik, H. A. Atwater, S. Meltzer, E. Harel, B. E. Koel, and A. A. G. Requicha, "Local detection of electromagnetic energy transport below the diffraction limit in metal nanoparticle Plasmon waveguides," *Nature Materials*, vol. 2, pp. 229–232, Apr. 2003.

[6] J. A. Dionne, L. A. Sweatlock, H. A. Atwater, and A. Polman, "Plasmon slot waveguides: Toward chip-scale propagation with subwavelength-scale localization," *Phys. Rev. B*, vol. 73, pp. 035407-1–035407-9, 2006.

[7] Q. Zhang, X. Haung, X. Lin, J. Tao, and X. Jin, "A subwavelength coupler-type MIM optical filter," *Optics Express*, vol. 19, pp. 2548–2554, Apr. 2009.

[8] A. Hosseini and M. Yehia, "Nanoscale surface plasmon based resonator using rectangular geometry," *Appl. Phys. Lett.*, vol. 90, pp. 181102-3–181102-3, Apr. 2007.

[9] C. Min and G. Veronis, "Absorption switches in metal-insulator-metal plasmonic waveguides," *Optics Express*, vol. 17, pp. 10757–10766, Jun. 2009.

[10] M. Pu, N. Yao, C. Hu, X. Xin, Z. Zhau, C. Wang, and X. Luo, "Directional coupler and nonlinear Mach-Zehnder intrerferometer based on metal-insulator-metal plasmonic waveguide," *Optics Express*, vol. 18, pp. 21030–21037, Sep. 2010.

[11] R. A. Wahsheh, Z. lu, and M. A. G. Aboushagur, "Nanoplasmonic directional couplers and Mach-Zehnder interferometers," *Optics Commun.*, vol. 282, pp. 4622–4626, Aug. 2009.

[12] N. Nozhat and N. Granpayeh, "Analysis of the plasmonic power splitter and MUX/DEMUX suitable for photonic integrated circuit," *Optics Commun.*, vol. 284, pp. 3449–3455, Mar. 2011.

[13] A. A. Reiserer, J. Haung, B. Hecht, and T. Brixner, "Subwavelength broadband splitter and switches for femtosecond plasmonic signal," *Optics Express*, vol. 18, pp. 11810–11820, May 2010.

[14] H. T. Miyazaki and Y. Kurokawa, "Squeezing visible light waves into a 3-nm-thick and 55-nm-long plasmon cavity," *Phys. Rev. Lett.*, vol. 96, pp. 097401-1–097401-4, Mar. 2006.

[15] I. Hyungsoon, C. B. Kyle, C. L. Nathan, L. H. Christy, and O. Sang-Hyun, "Vertically oriented sub-10-nm plasmonic nanogap arrays," *Nano Lett.*, vol. 10, pp. 2231–2236, May 2010.

[16] D. S. Ly-Gangon, S. E. Kocabas, and D. A. B. Miller, "Characteristic impedance model for plasmonic metal slot waveguides," *IEEE J. Sel. Topics Quantum Electron.*, vol. 14, no. 6, pp. 1473–1478, Nov. 2008.

[17] A. Pannipitiya, I. D. Rukhlenko, and M. Premaratne, "Analytical modeling of resonant cavities plasmonic-slot-waveguide junctions," *IEEE Photon. J.*, vol. 3, no. 2, pp. 220–233, Apr. 2011.

[18] A. Pannipitiya, I. D. Rukhlenko, M. Premaratne, H. T. Hattori, and G. P. Agrawal, "Improved transmission model for metal-dielectric-metal plasmonic waveguides with stub structure," *Optics Express*, vol. 18, pp. 6191–6204, Mar. 2010.

[19] G. Veronis and S. Fan, "Bends and splitters in metal-dielectric-metal subwavelength plasmonic waveguides," *Appl. Phys. Lett.*, vol. 87, pp. 131102-1–131102-3, Sep. 2005.

[20] S. E. Kocabas, G. Veronis, D. A. B. Miller, and S. Fan, "Transmission line and equivalent circuits models for plasmonic waveguide components," *IEEE J. Sel. Topics Quantum Electron.*, vol. 14, no. 6, pp. 1462–1472, Nov. 2008.

[21] Y. Xu, A. E. Miroshnichenko, S. Lan, Q. Guo, and L. Wu, "Impedance matching induce high transmission and flat response band-pass plasmonic waveguides," *Plasmonics*, vol. 6, pp. 337–343, Feb. 2011.

[22] M. Rezaei, M. Miri, A. Khavasi, K. Mehrany, and B. Rashidian, "An efficient circuit model for the analysis and design of rectangular plasmonic resonator," *Plasmonics*, [Online]. Available: http://dx.doi.org/10.1007/s11468-011-9300-x

[23] C. Chen, P. Berini, D. Feng, S. Tanev, and V. Tzolov, "Efficient and accurate numerical analysis of multilayer planar optical waveguides in lossy anisotropic media," *Optics Express*, vol. 7, pp. 260–272, Oct. 2000.

Mohsen Rezaei was born in Razan, Hamedan, Iran, on April 25, 1986. He received the B.Sc. degree from the University of Tehran, Iran, in 2008, and the M.Sc. degree from the Sharif University of Technology, Tehran, Iran, in 2011, both in electrical engineering.

Since spring 2010, he has been a Research Assistant at the Integrated Photonic Laboratory at the Sharif University of Technology. His research interests include photonics, plasmonics and nonlinear optics.

Sadegh Jalaly was born in Isfahan, Iran, on June 25, 1986. He received the B.Sc. degree in electrical engineering from the Isfahan University of Technology, Isfahan, Iran, in 2009. Currently, he is working toward the M.Sc. degree in the Department of Electrical Engineering, Sharif University of Technology, Tehran, Iran.

His research interests include photonics, optical resonators, and computational electromagnetics.

Mehdi Miri was born in Shiraz, Iran, on October 26, 1983. He received the B.Sc. degree in electrical engineering from Shiraz University, Shiraz, Iran, in 2006, and the M.Sc. degree in electronics engineering from the Sharif University of Technology, Tehran, Iran, in 2008, where he is currently working toward the Ph.D. degree in electrical engineering.

His research interests include photonic crystals, numerical methods, and quantum optics.

Amin Khavasi was born in Zanjan, Iran, on January 22, 1984. He received the B.Sc. and M.Sc. degrees from the Sharif University of Technology, Tehran, Iran, in 2006 and 2008, respectively, both in electrical engineering. He is currently working toward the Ph.D. degree in the same university.

His research interest include photonics, circuit modeling of photonic structures, and computational electromagnetic.

Ali P. Fard was born in Isfahan, Iran, on April 9, 1986. He received the B.Sc. degree in the Department of Electrical and Computer Engineering, University of Tehran, Iran, in 2009. Currently, he is working toward the M.Sc. degree in the Department of Electrical Engineering, Sharif University of Technology, Tehran, Iran.

Since spring 2010, he has been a Research Assistant at the Integrated Photonic Laboratory at the Sharif University of Technology. His research interests include all optical systems, fiber-optic communication, optical isolation and nonlinear optics.

Khashayar Mehrany was born in Tehran, Iran, on September 16, 1977. He received the B.Sc., M.Sc., and Ph.D. (*magna cum laude*) degrees from the Sharif University of Technology, Tehran, Iran, in 1999, 2001, and 2005, respectively, all in electrical engineering.

Since then, he has been an Associate Professor with the Department of Electrical Engineering, Sharif University of Technology. His current research interests include photonics, plasmonics, and intergral imaging.

Bizhan Rashidian received the B.Sc. and M.Sc. (Hons.) degrees from Tehran University,Tehran, Iran, in 1987 and 1989, respectively, and the Ph.D. degree from the Georgia Institute of Technology, Atlanta, in 1993, all in electrical engineering.

Since 1994, he has been with the Department of Electrical Engineering, Sharif University of Technology, Tehran, Iran, where he is currently a Professor. He is also the Founding Director of the Microtechnology Laboratory, Nanoelectronics Laboratory, and the Photonics Laboratory. His active research areas include optics, nanoelectronics, micromachining, microelectronics, and ultrasonic.